

Controllable Synthesis of NiCo₂O₄/CNT Composites for Supercapacitor Electrode Materials

Yanhua Li*, Lei Zheng, Wanyin Wang, Yuexuan Wen

Hunan Province Key Laboratory of Applied Environmental Photocatalysis, Changsha University, Changsha 410022, China

*E-mail: liyanhua11@126.com

Received: 7 July 2020 / *Accepted:* 31 August 2020 / *Published:* 30 September 2020

NiCo₂O₄/CNT composites were obtained by a hydrothermal process through changing the content of sodium dodecyl sulfate (SDS), followed by an annealing treatment. The addition of different content of SDS affects the morphology, the structure and the capacitive characteristics of NiCo₂O₄/CNT composites. In comparison with NiCo₂O₄/CNT composite synthesized without the addition of SDS, the specific capacitance of NiCo₂O₄/CNT composites prepared with the addition of 0.288, 0.576, 0.864, and 1.152 g of SDS can be increased in different degree. Among them, NiCo₂O₄/CNT composite synthesized with the addition of 0.864 g of SDS exhibits the highest specific capacitance. Its specific capacitance at 0.5 A g⁻¹ is 574.3 F g⁻¹, which is 2.01 times as large as that of NiCo₂O₄/CNT composite synthesized without the addition of SDS. Besides, NiCo₂O₄/CNT composite with the addition of 0.864 g of SDS exhibits the specific capacitance retention of 75.3% at 8 A g⁻¹ and initial specific capacitance retention of 111.5% after 1000 cycles, indicating good rate performance and superb cycle performance. All these characteristics demonstrate that NiCo₂O₄/CNT composite with the addition of 0.864 g of SDS is a promising supercapacitor electrode material.

Keywords: Supercapacitors; NiCo₂O₄; CNT; Composite

1. INTRODUCTION

With the increasing energy crisis, environmental pollution and global warming, the development of sustainable and renewable energy storage systems has stimulated growing research interest [1]. As energy storage systems, supercapacitors can provide longer cycle life and larger power output than batteries [2]. They have been applied in various mobile electronic devices and hybrid electric vehicles. According to energy storage mechanisms, supercapacitors can be classified into two types: electrical double layer capacitors and pseudocapacitors [3]. Electrical double layer capacitors store charges arising from ions adsorption at the electrode–electrolyte interface. Pseudocapacitors store charges mainly

relying on faradaic redox reactions at the vicinity of the surface [4]. The electrode materials play an important role in determining the performance of supercapacitors. Carbon materials [5, 6], transition metal oxides [7-9], and conducting polymers [10] have been investigated widely and extensively in supercapacitors.

As a mixed transition metal oxides, NiCo_2O_4 has advantages in inexpensiveness, environmental friendliness and natural abundance. Besides, the electrical conductivity and electrochemical activity of NiCo_2O_4 is better than that of pure NiO or Co_3O_4 [11, 12]. These intriguing features make NiCo_2O_4 to be used as electrode material for supercapacitors [1]. Various NiCo_2O_4 materials with diverse morphologies, such as nanoneedles [13], nanosheets [14], nanowires [15], nanoflower [16], and hollow spheres [17] have been obtained using different synthesis methods including hydrothermal reactions, sol-gel method and electrodeposition process. NiCo_2O_4 materials with different morphologies exhibit different capacitive performance. However, the conductivity of NiCo_2O_4 is still not high enough for fast transfer of electrons, leading to the capacitance contribution restrained at the vicinity of the material surface and poor cycle stability [18, 19]. As a result, its applications in high-performance supercapacitors is limited.

To overcome aforementioned shortcomings, an effective strategy is to form composites by combining NiCo_2O_4 with carbon materials since carbon materials can improve the electric conductivity. Among carbon materials, carbon nanotubes (CNT) exhibit multiple advantages such as remarkable conductivity, high specific surface areas, excellent flexibility, good thermal and chemical stability [1921]. Up to now, several studies on $\text{NiCo}_2\text{O}_4/\text{CNT}$ composites for supercapacitors have been reported [19-27]. However, in their researches, $\text{NiCo}_2\text{O}_4/\text{CNT}$ composites were usually synthesized with twostep processes, which involved the preparation of CNT and the synthesis of $\text{NiCo}_2\text{O}_4/\text{CNT}$ composites. Besides, there have been no reports on controllable synthesis of $\text{NiCo}_2\text{O}_4/\text{CNT}$ composites for supercapacitor electrodes. In our previous work [28], the morphology of NiCo_2O_4 was controlled in the process of hydrothermal synthesis through changing types of surfactants (without any surfactants, 0.6 g of Triton X-100, 0.6 g of cetyl trimethyl ammonium bromide, 0.6 g of sodium dodecyl sulfate) and the influence of different surfactants on the capacitive performance of NiCo_2O_4 was studied. The addition of sodium dodecyl sulfate can greatly affect the morphology of NiCo_2O_4 , thus improving its specific capacitance and cycle performance.

In the present work, $\text{NiCo}_2\text{O}_4/\text{CNT}$ composites with different morphologies and structures were obtained by a one-step hydrothermal synthesis with the addition of different amount (0, 0.288, 0.576, 0.864, 1.152 g) of sodium dodecyl sulfate (SDS). The addition of different amount of SDS has impact on the morphology and the structure of NiCo_2O_4 in $\text{NiCo}_2\text{O}_4/\text{CNT}$ composites, thereby leading to different capacitive property of $\text{NiCo}_2\text{O}_4/\text{CNT}$ composites. In comparison with $\text{NiCo}_2\text{O}_4/\text{CNT}$ composite synthesized without any SDS, $\text{NiCo}_2\text{O}_4/\text{CNT}$ composite obtained by adding SDS displays larger specific capacitance. Among them, $\text{NiCo}_2\text{O}_4/\text{CNT}$ composite obtained with the addition of 0.864 g of SDS shows the highest specific capacitance. Moreover, it presents good rate performance and superior cycle performance. Finally, this work also provides an available method to enhance the capacitive characteristics of mixed transition metal oxides/CNT composite for supercapacitor electrode.

2. EXPERIMENTAL

2.1. Preparation of NiCo₂O₄/CNT composites

NiCo₂O₄/CNT composites were synthesized by a one-step hydrothermal method with the addition of different amount of SDS, followed by an annealing treatment. The synthetic process was depicted as follows. 160 mg of CNT was ultrasonically dispersed in 60 mL deionized water. Then, 0.582 g of Ni(NO₃)₂·6H₂O, 1.164 g of Co(NO₃)₂·6H₂O, 1.8 g of CO(NH₂)₂, and 0.444 g of NH₄F were added into above suspension under stirring. After that, the obtained mixture was poured into a 100 mL Teflonlined autoclave, sealed and kept at 150 °C for 8 h in the oven. After the autoclave was cooled down to room temperature naturally, the prepared solid materials were washed with deionized water and ethanol for 3 times, and then dried at 60 °C for 12 h in the oven. Finally, NiCo₂O₄/CNT composite, denoted as NiCo₂O₄/CNT-1, was obtained by calcining the dried solid materials at 350 °C for 3 h. Under the same condition, NiCo₂O₄/CNT composites synthesized with the addition of 0.288 g, 0.576 g, 0.864 g, and 1.152 g of SDS were designated as NiCo₂O₄/CNT-2, NiCo₂O₄/CNT-3, NiCo₂O₄/CNT-4, and NiCo₂O₄/CNT-5, respectively.

2.2. Materials Characterization

The crystal structures of the synthesized composites were recorded by X-ray diffraction (XRD, Rigaku D/max 2550) with Cu K α radiation. The sizes and morphologies of the composites were observed by scanning electron microscopy (SEM, FEI quanta FEG 400) and transmission electron microscopy (TEM, FEI Tecnai G2 F20). N₂ adsorption-desorption isotherms were measured by Brunauer-EmmettTeller (BET, Quantachrome Instruments Quadrasorb EVO) measurements. The pore size distributions were obtained by applying the Barrett-Joyner-Halenda (BJH) equation. Existing elements and their valence states were carried out with X-ray photoelectron spectroscopy (XPS, Escalab 250Xi, USA) with monochromated Al K α radiation.

2.3. Electrochemical measurements

Cyclic voltammetry (CV), chronopotentiometry (CP), and electrochemical impedance spectroscopy (EIS) were conducted with a CHI 660E electrochemical workstation in 2 M KOH solution electrolyte. The slurry was obtained by mixing NiCo₂O₄/CNT composite (75 wt %), acetylene black (20 wt %), and polytetrafluoroethylene (5 wt %). Then, the obtained-slurry was coated on a nickel foam. The coated nickel foam was pressed at 15 MPa and dried under vacuum at 110 °C for 12 h to obtain the working electrode. A platinum plate and a saturated calomel electrode (SCE) were used as the counter and reference electrodes, respectively. EIS measurements were made in the frequency range from 0.01 to 10⁵ Hz.

3. RESULTS AND DISCUSSION

3.1. Structural characteristics

Fig. 1 shows XRD patterns of NiCo₂O₄/CNT-1, NiCo₂O₄/CNT-2, NiCo₂O₄/CNT-3, NiCo₂O₄/CNT-4, and NiCo₂O₄/CNT-5.

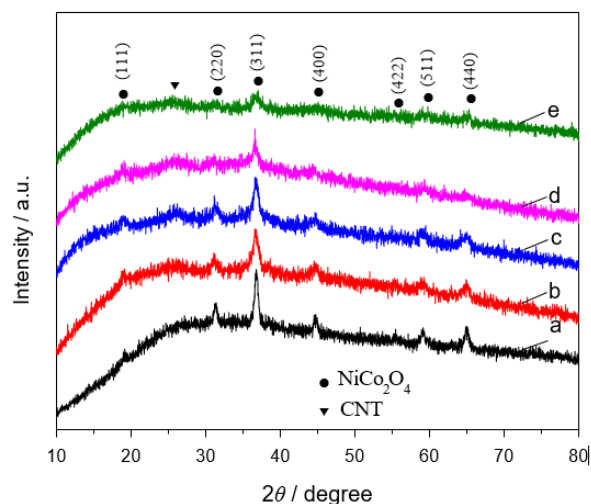
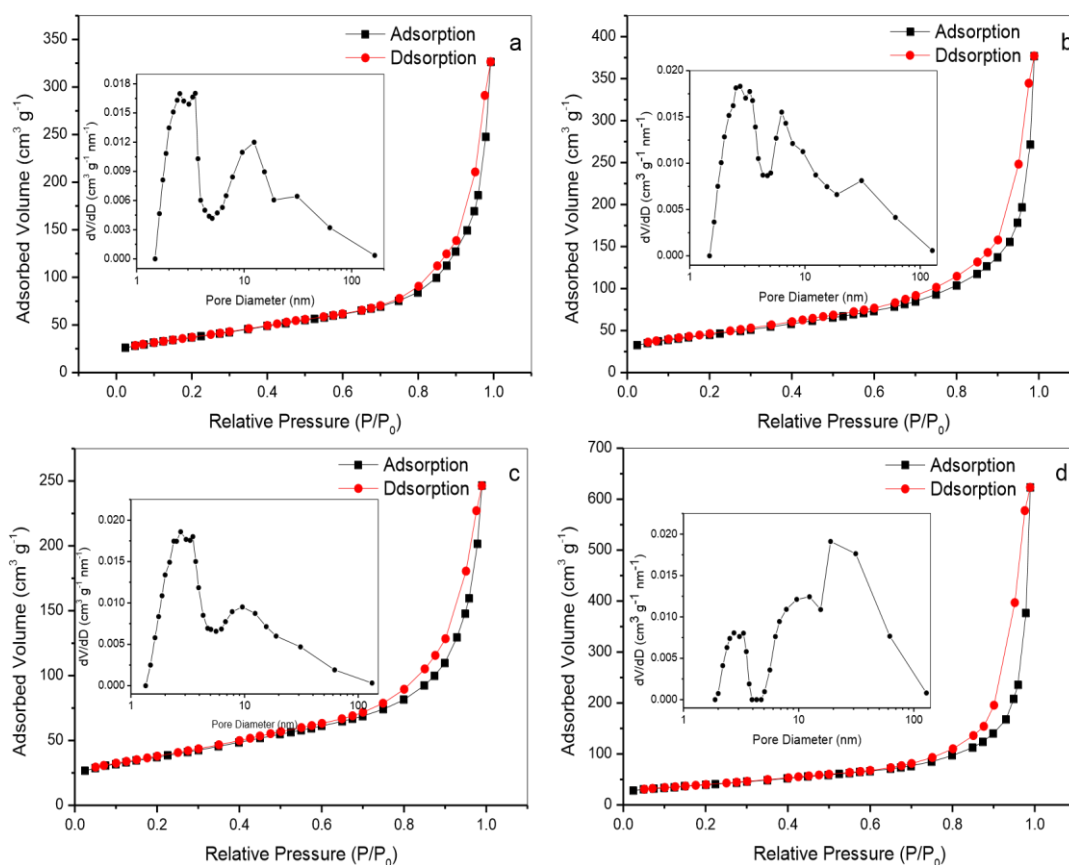


Figure 1. XRD patterns of NiCo₂O₄/CNT-1 (a), NiCo₂O₄/CNT-2 (b), NiCo₂O₄/CNT-3 (c), NiCo₂O₄/CNT-4 (d), and NiCo₂O₄/CNT-5 (e).



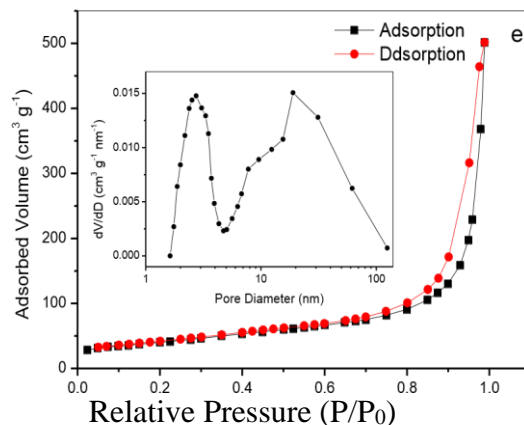


Figure 2. Nitrogen adsorption-desorption and pore size distribution curves (inset) of NiCo₂O₄/CNT-1 (a), NiCo₂O₄/CNT-2 (b), NiCo₂O₄/CNT-3 (c), NiCo₂O₄/CNT-4 (d), and NiCo₂O₄/CNT-5 (e).

The XRD peaks observed at 19.0°, 31.2°, 36.8°, 44.8°, 55.8°, 59.1°, and 65.0° are attributed to the (111), (220), (311), (400), (422), (511), and (440) crystal planes of the cubic phase NiCo₂O₄ (JCPDS No.20-0781). A weakened diffraction peak at around 26° corresponds to the (002) plane of CNT. No impurity peaks are observed, implying that all the synthesized-samples are NiCo₂O₄/CNT composites.

The positions of the characteristic peaks in all the NiCo₂O₄/CNT composites are consistent. However, except for weakened diffraction peak at around 26° indexed to the characteristic peak of CNT, the other peaks width at half maxima intensity rank from high to low as follows: NiCo₂O₄/CNT-1, NiCo₂O₄/CNT-2, NiCo₂O₄/CNT-3, NiCo₂O₄/CNT-4, NiCo₂O₄/CNT-5. The peak width at half maxima intensity demonstrates that NiCo₂O₄ in NiCo₂O₄/CNT composite exhibits small crystallite size. Therefore, the order of the crystallite size from large to small is as follows: NiCo₂O₄ in NiCo₂O₄/CNT1, NiCo₂O₄ in NiCo₂O₄/CNT-2, NiCo₂O₄ in NiCo₂O₄/CNT-3, NiCo₂O₄ in NiCo₂O₄/CNT-4, NiCo₂O₄ in NiCo₂O₄/CNT-5. This implies that the crystallite size of NiCo₂O₄ in NiCo₂O₄/CNT composite decreases with the increase of the addition amount of SDS.

Fig. 2 displays nitrogen adsorption-desorption and corresponding pore size distribution curves as inset of NiCo₂O₄/CNT-1, NiCo₂O₄/CNT-2, NiCo₂O₄/CNT-3, NiCo₂O₄/CNT-4, and NiCo₂O₄/CNT-5. The specific surface areas of NiCo₂O₄/CNT-1, NiCo₂O₄/CNT-2, NiCo₂O₄/CNT-3, NiCo₂O₄/CNT-4, and NiCo₂O₄/CNT-5 are 132.2, 158.3, 131.6, 141.2, 143.6 m²g⁻¹, respectively. Among five NiCo₂O₄/CNT composites, the specific surface areas of NiCo₂O₄/CNT-1 and NiCo₂O₄/CNT-3 are almost the same, exhibiting the lowest value. However, for five composites, there are no significant difference in specific surface area. All the composites show a typical type IV isotherm with a typical H3 hysteresis loop, implying mesoporous nature. Average pore diameter of NiCo₂O₄/CNT-1, NiCo₂O₄/CNT-2, NiCo₂O₄/CNT-3, NiCo₂O₄/CNT-4, and NiCo₂O₄/CNT-5 are 15.29, 14.74, 11.58, 27.32, and 21.61 nm, respectively. The above analysis shows that the specific surface area of NiCo₂O₄/CNT-4 is not the highest.

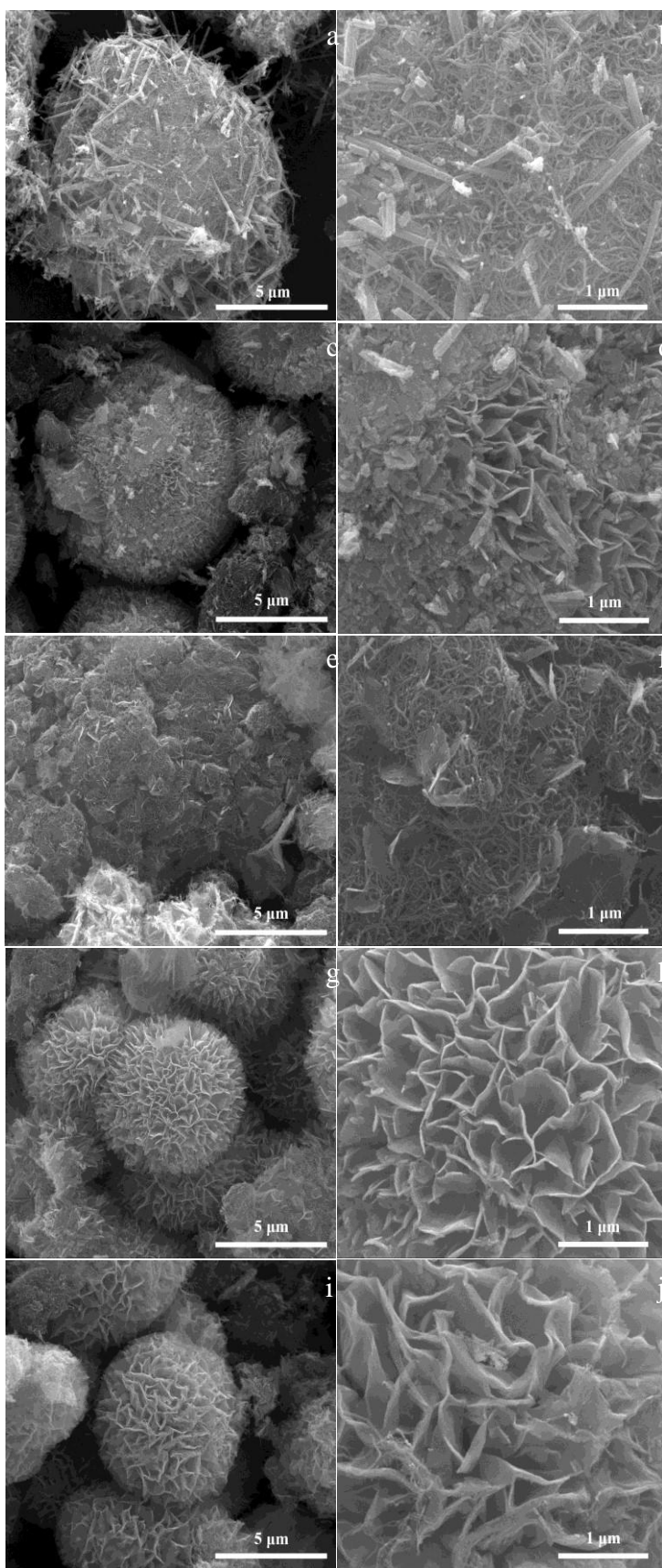


Figure 3. SEM images of NiCo₂O₄/CNT-1 (a, b), NiCo₂O₄/CNT-2 (c, d), NiCo₂O₄/CNT-3 (e, f), NiCo₂O₄/CNT-4 (g, h), and NiCo₂O₄/CNT-5 (i, j).

However, it exhibits the largest average pore diameter, which is significantly larger than that of the other composites. This can be easily more desirable for the penetration of electrolytes and reactant into the whole electrode, thus possessing best specific capacitance.

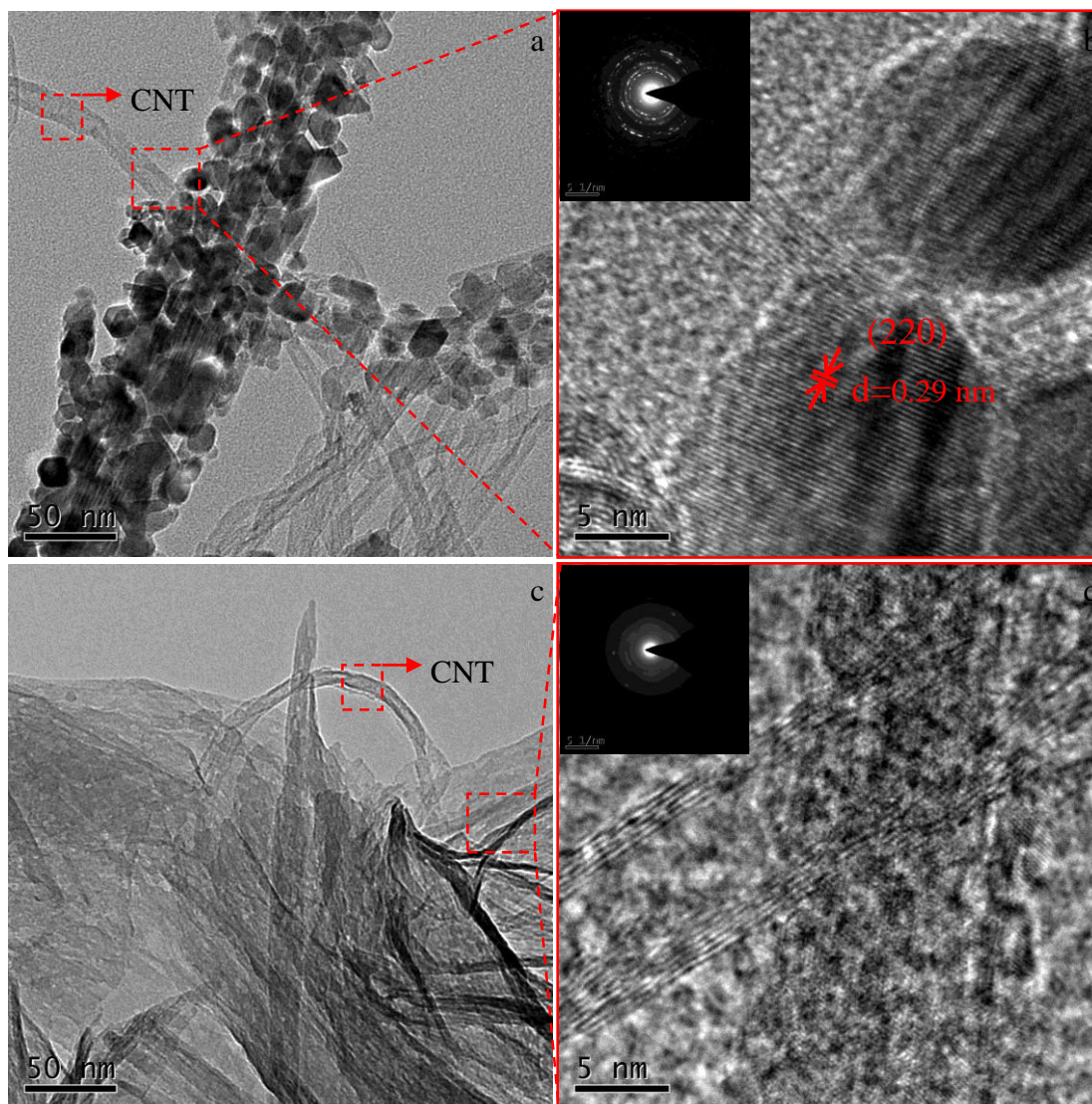


Figure 4. TEM images of NiCo₂O₄/CNT-1 (a) and NiCo₂O₄/CNT-4 (b), HRTEM images of images of NiCo₂O₄/CNT-1 (c) and NiCo₂O₄/CNT-4 (d). The inset is the corresponding SAED pattern.

The morphologies and microstructures of the as-synthesized composites were investigated by SEM, TEM and HRTEM. SEM images of NiCo₂O₄/CNT-1, NiCo₂O₄/CNT-2, NiCo₂O₄/CNT-3, NiCo₂O₄/CNT-4, and NiCo₂O₄/CNT-5 are shown in Fig. 3. TEM images, HRTEM images and corresponding selected-area electron diffraction (SAED) patterns of NiCo₂O₄/CNT-1 and NiCo₂O₄/CNT-4 are displayed in Fig. 4. As shown in Fig. 3a and 3b, the morphology of NiCo₂O₄/CNT1 composites consists of a great number of CNTs and a certain number of NiCo₂O₄ nanocorns. More detailed structural information and morphology of NiCo₂O₄/CNT-1 are shown in Fig. 4a and 4b.

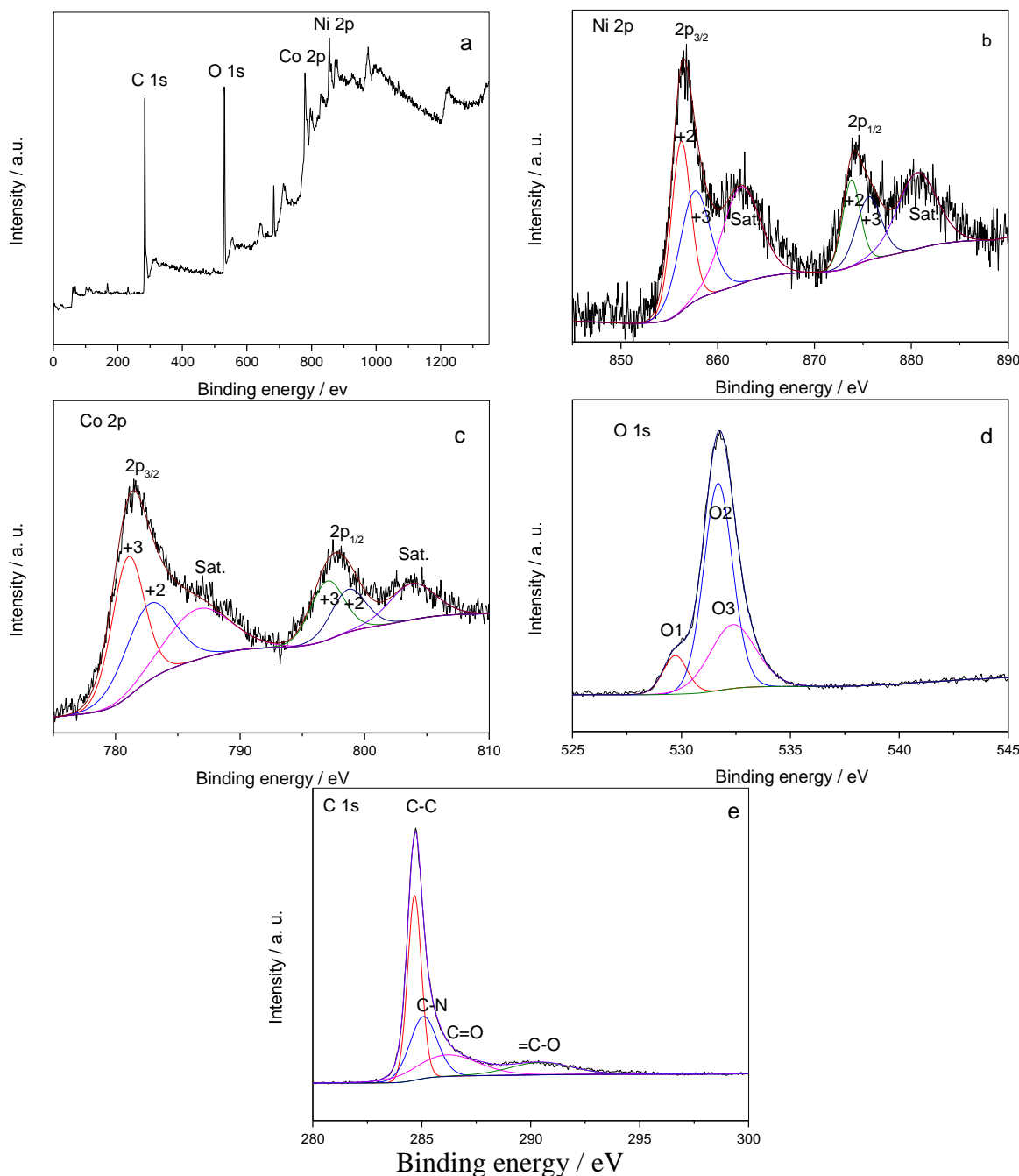


Figure 5. XPS spectra of NiCo₂O₄/CNT-4: (a) survey spectrum, (b) Ni 2p, (c) Co 2p, (c) O 1s, and (e) C 1s.

CNT marked by red dotted box and NiCo₂O₄ nanocorns consisting of particles with a diameter of 13-15 nm clearly are observed in Fig. 4a. According to HRTEM (Fig. 4b), the lattice space of 0.29 nm corresponds to the (220) plane of NiCo₂O₄. SAED pattern (inset of Fig. 4b) exhibits a series of concentric rings, indicating the polycrystalline structure of NiCo₂O₄. As observed in Fig. 3c and 3d, the morphology of NiCo₂O₄/CNT-2 is microspheres, which consists of NiCo₂O₄ nanoflakes and nanocorn. Microspheres are twined by a small amount of CNT.

Besides, a certain number of CNT is observed in NiCo₂O₄/CNT-2. For NiCo₂O₄/CNT-3 (Fig. 3e and 3f), a number of CNT and NiCo₂O₄ nanoflakes are observed. NiCo₂O₄ nanoflakes are isolated by a

number of CNT. Moreover, a few of NiCo₂O₄ nanocorn is also found. For NiCo₂O₄/CNT-4 (Fig. 3g and Fig. 3h) and NiCo₂O₄/CNT-5 (Fig. 3i and Fig. 3j), NiCo₂O₄ with the morphology of flower-shaped microspheres constructed by intercross nanoflakes is observed and NiCo₂O₄ with the morphology of nanocorn disappears. A few of CNT is observed in NiCo₂O₄/CNT-4 and NiCo₂O₄/CNT-5. However, the majority of CNT is wrapped in NiCo₂O₄ flower-shaped microspheres of NiCo₂O₄/CNT-4 and NiCo₂O₄/CNT-5. A major difference in NiCo₂O₄/CNT-4 and NiCo₂O₄/CNT-5 is that thinner NiCo₂O₄ nanoflakes constituting flower-shaped microspheres exist in NiCo₂O₄/CNT-5. Fig. 4c and 4d display detailed structural information and morphology of CNT and NiCo₂O₄ in NiCo₂O₄/CNT-4. HRTEM (Fig. 4d) clearly shows that the lattice phase of NiCo₂O₄ has random orientation the lattice. SAED pattern (inset of Fig. 4d) shows a set of well-defined concentric rings, indicating the polycrystalline structure of NiCo₂O₄.

Existing elements and their valence states were characterized by XPS. Fig. 5 show that XPS spectra of NiCo₂O₄/CNT-4. The survey spectrum (Fig. 5a) indicates the presence of Ni, Co, O, and C in NiCo₂O₄/CNT-4. Figure 5b, 5c, 5d, and 5e depict the high resolution spectra of Ni 2p, Co 2p, O 1s, and C 1s, respectively. By using Gaussian fitting method, Ni 2p spectrum and Co 2p spectrum can be fitted as two spin-orbit doublets and two satellites (denoted as "Sat."). In Fig. 5b, the fitting peaks at 856.2 and 873.8 eV are attributed to Ni²⁺, and those at 857.6 and 875.6 eV are assigned to Ni³⁺. The two satellite peaks are observed at 862.0 and 880.3 eV, which refer to shakeup peaks of Ni species. In Fig. 5c, the fitting peaks at 782.7 and 798.7 eV are assigned to Co²⁺, and those at 781 and 796.98 eV are indexed to Co³⁺. The satellite peaks at 785.4 and 803.8 eV are ascribed to shakeup peaks of Co species [29]. As showed in Fig. 5d, the high resolution spectrum of O 1s can be divided into three oxygen contributions labeled as O₁, O₂, and O₃. The O₁ component at 529.74 eV can be attributed to a typical metal–oxygen bond [30], while the O₂ component at 531.69 eV corresponds to defect sites [12, 17]. The O₃ component at 532.36 eV can be due to multiplicity of chemisorbed and physisorbed water on the surface [12, 17]. The high resolution spectrum of C 1s (Fig. 5e) shows four peaks located at 284.67, 285.08, 286.17 and 290.45 eV, corresponding to the carbon bonds in C-C, C-N, C=O and O=C-O, respectively [23, 30]. XPS results verify that the presence of Ni²⁺, Ni³⁺, Co²⁺, and Co³⁺ come from NiCo₂O₄, which is in accordance with the literatures [12, 17, 29]. Meanwhile, XPS results also confirm C element from CNT.

3.2. Electrochemical capacitor property

Cyclic voltammograms of NiCo₂O₄/CNT-4 NiCo₂O₄/CNT-1, NiCo₂O₄/CNT-2, NiCo₂O₄/CNT3 NiCo₂O₄/CNT-4 and NiCo₂O₄/CNT-5 at different scan rates is presented in Fig. 6a-6e. The peak current density and the integrated CV area gradually become larger when the scan rate increases from 5 to 40 mV s⁻¹. In addition, the anodic and cathodic peaks move toward higher potential and lower potential when increasing the scan rate, respectively. This is interpreted based on the polarization effect of the electrode.

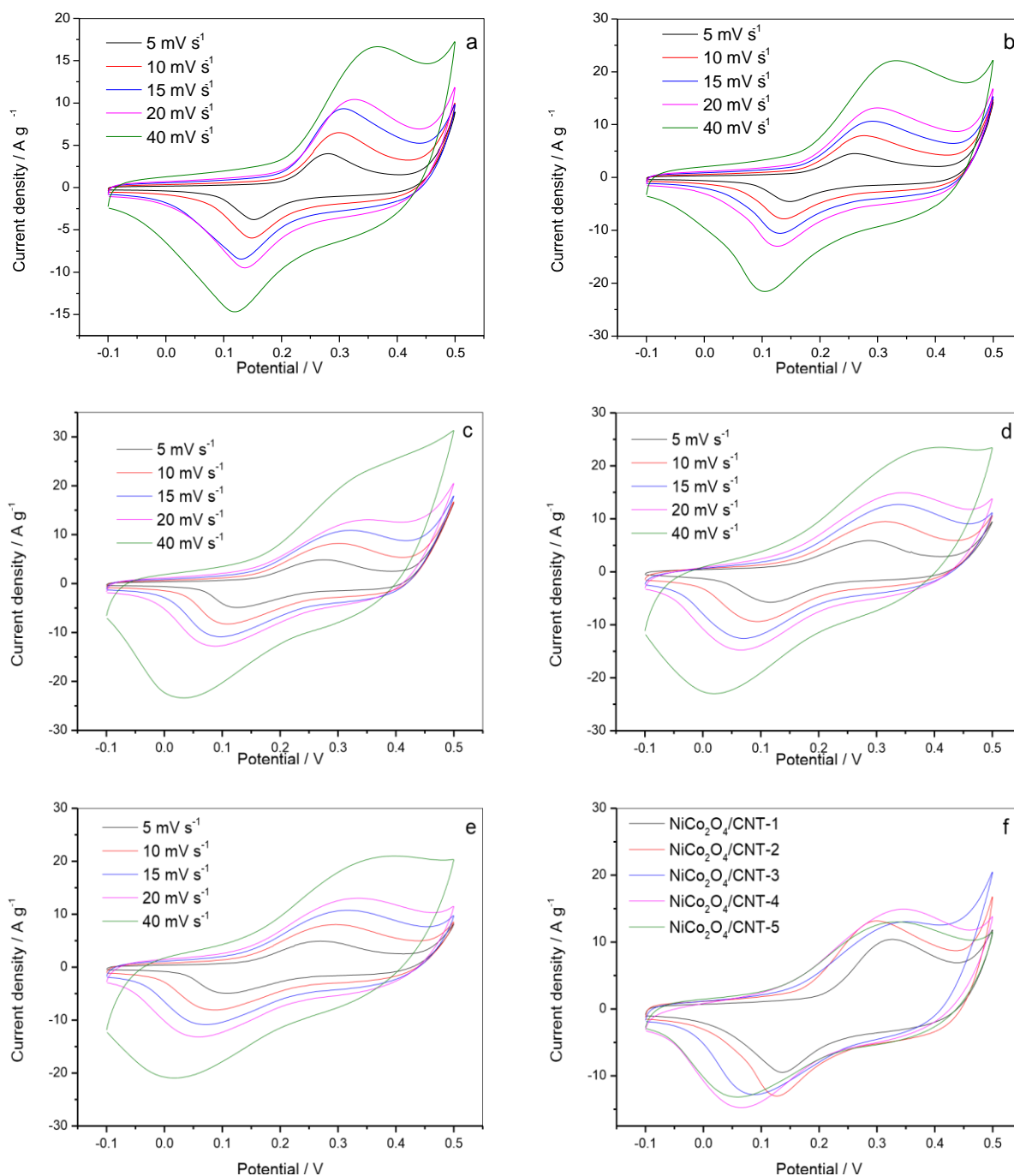
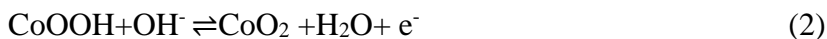


Figure 6. Cyclic voltammograms of NiCo₂O₄/CNT-4 NiCo₂O₄/CNT-1 (a), NiCo₂O₄/CNT-2 (b), NiCo₂O₄/CNT-3 (c), NiCo₂O₄/CNT-4 (d), and NiCo₂O₄/CNT-5 (e) at scan rates of 5, 10, 15, 20, and 40 mV s⁻¹; Cyclic voltammograms of NiCo₂O₄/CNT-1, NiCo₂O₄/CNT-2, NiCo₂O₄/CNT-3, NiCo₂O₄/CNT-4, and NiCo₂O₄/CNT-5 at a scan rate of 20 mV s⁻¹ (f);

Fig. 6f shows cyclic voltammograms of NiCo₂O₄/CNT-1, NiCo₂O₄/CNT-2, NiCo₂O₄/CNT-3, NiCo₂O₄/CNT-4, and NiCo₂O₄/CNT-5 at a scan rate of 20 mV s⁻¹ in potential range from -0.1 to 0.5 V.

The shape of the CV curves is not an ideal rectangular shape but presents distinct redox peaks, demonstrating that capacitance mainly derives from pseudo-capacitance caused by faradaic redox reactions. A couple of redox peaks are observed and correspond to the following reactions.



Five NiCo₂O₄/CNT composites present different integrated CV areas, indicating that they possess different the specific capacitance. Among them, the integrated CV area ranks from high to low as follows: NiCo₂O₄/CNT-4, NiCo₂O₄/CNT-5, NiCo₂O₄/CNT-3, NiCo₂O₄/CNT-2, NiCo₂O₄/CNT-1. The larger the integrated CV areas, the higher the specific capacitance. Therefore, the order of the specific capacitance is NiCo₂O₄/CNT-4 > NiCo₂O₄/CNT-5 > NiCo₂O₄/CNT-3 > NiCo₂O₄/CNT-2 > NiCo₂O₄/CNT-1. This may be ascribable to different NiCo₂O₄ crystallite sizes, NiCo₂O₄ morphologies, the specific surface areas and the average pore diameters. NiCo₂O₄/CNT-4 possesses the highest specific capacitance, which can be explained as follows. Although the specific surface area of NiCo₂O₄/CNT-4 is not the highest (the third highest) and NiCo₂O₄ crystallite size of NiCo₂O₄/CNT-4 is not the smallest (the second smallest). NiCo₂O₄/CNT-4 possesses the largest average pore diameter, which may be more appropriate for the penetration of electrolytes and reactant into the whole electrode. Besides, NiCo₂O₄ morphology of NiCo₂O₄/CNT-4 is nanoflakes constituting flower-shaped microspheres and the majority of CNT are wrapped in NiCo₂O₄ flower-shaped microspheres. This may be beneficial to mass transportation and electrode conduction [31]. NiCo₂O₄/CNT-1 exhibits the lowest specific capacitance. This owes to the largest NiCo₂O₄ crystallite size and the lowest specific surface area. Moreover, a certain number of NiCo₂O₄ nanocorns consisting of particles are observed in NiCo₂O₄/CNT-1. NiCo₂O₄ nanocorns may be adverse to mass transportation and electrode conduction when compared with NiCo₂O₄ flower-shaped microspheres composed of nanoflakes.

Fig. 7a-7e depicts constant current charge/discharge curves of NiCo₂O₄/CNT-1, NiCo₂O₄/CNT2, NiCo₂O₄/CNT-3, NiCo₂O₄/CNT-4, and NiCo₂O₄/CNT-5 at different current densities. Fig. 7f shows constant current charge/discharge curves of NiCo₂O₄/CNT-1, NiCo₂O₄/CNT-2, NiCo₂O₄/CNT-3, NiCo₂O₄/CNT-4, and NiCo₂O₄/CNT-5 at the current density of 2 A g⁻¹. Nonlinearity in the chargedischarge curves shows the pseudocapacitive characteristics caused by Faradaic reactions. The specific capacitance of NiCo₂O₄/CNT-1, NiCo₂O₄/CNT-2, NiCo₂O₄/CNT-3, NiCo₂O₄/CNT-4, and NiCo₂O₄/CNT-5 can be calculated as follows [32-34].

$$C_{\text{sp}} = \frac{It}{mV} \quad (3)$$

where C_{sp} indicates the specific capacitance (F g⁻¹), I stands for the discharge current (A), t represents the discharge time (s), V denotes the potential range during the discharge, m is the mass of active material, respectively.

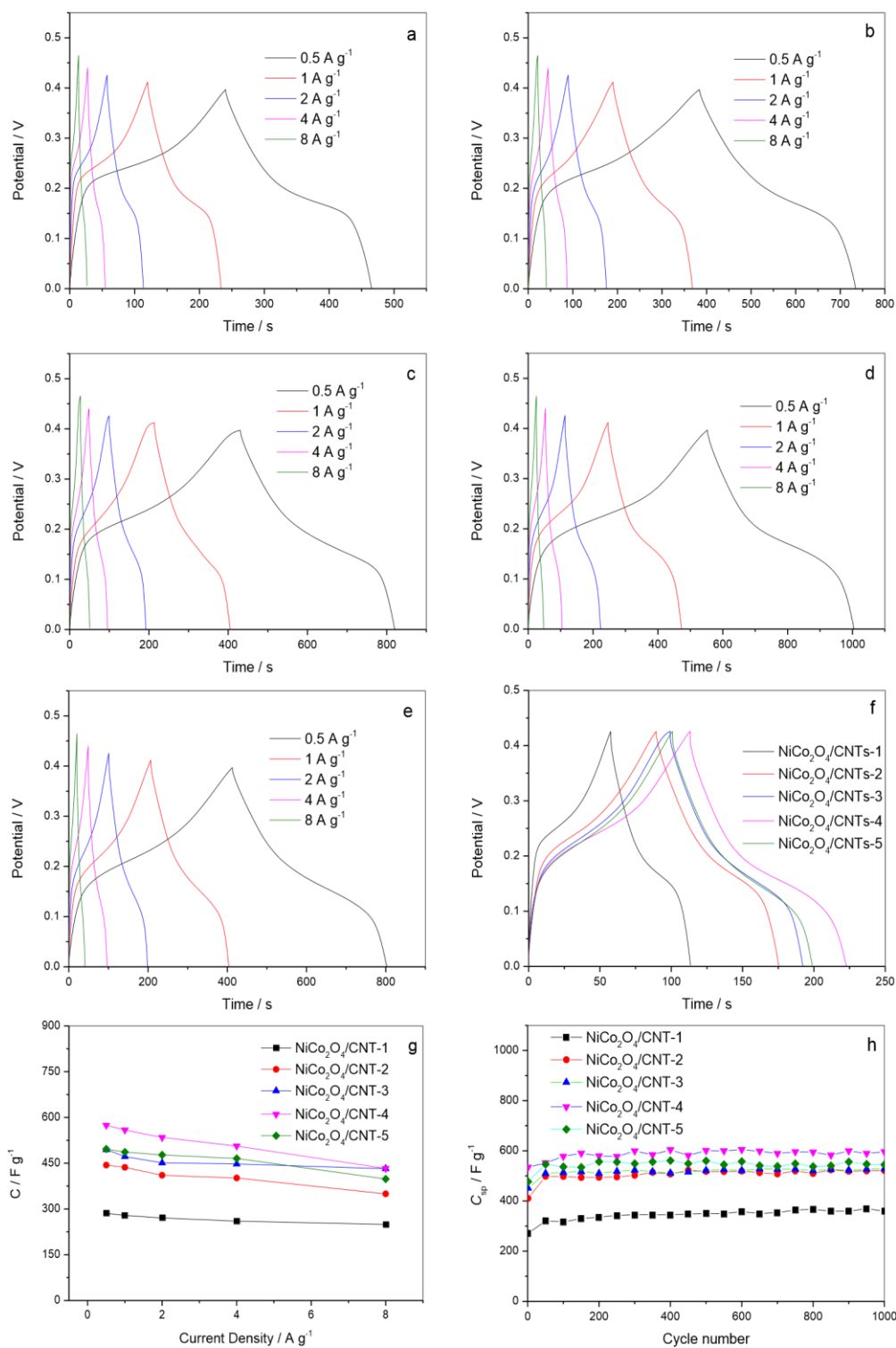
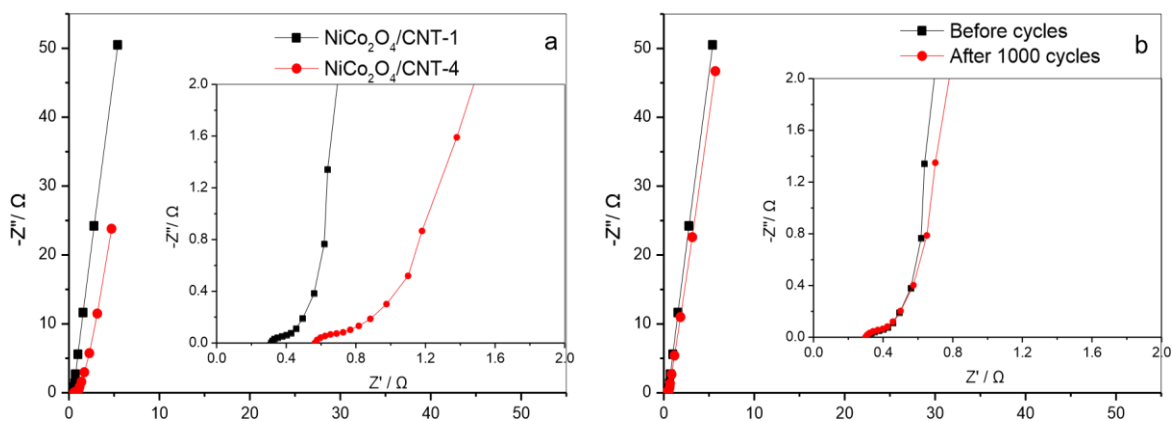


Figure 7. Constant current charge/discharge curves of NiCo₂O₄/CNT-1 (a), NiCo₂O₄/CNT-2 (b), NiCo₂O₄/CNT-3 (c), NiCo₂O₄/CNT-4 (d), and NiCo₂O₄/CNT-5 (e) at different current densities; Constant current charge/discharge curves of NiCo₂O₄/CNT-1, NiCo₂O₄/CNT-2, NiCo₂O₄/CNT-3, NiCo₂O₄/CNT-4, and NiCo₂O₄/CNT-5 at the current density of 2 A g⁻¹ (f); Relationship between the specific capacitance and the current density of NiCo₂O₄/CNT-1, NiCo₂O₄/CNT-2, NiCo₂O₄/CNT-3, NiCo₂O₄/CNT-4, and NiCo₂O₄/CNT-5 (g); Cycling performance of NiCo₂O₄/CNT-1, NiCo₂O₄/CNT-2, NiCo₂O₄/CNT-3, NiCo₂O₄/CNT-4, and NiCo₂O₄/CNT-5 at the current density of 2 A g⁻¹ (h).

Based on the equation (3), relationship between the specific capacitance and the current density of NiCo₂O₄/CNT-1, NiCo₂O₄/CNT-2, NiCo₂O₄/CNT-3, NiCo₂O₄/CNT-4, and NiCo₂O₄/CNT-5 is displayed in Fig. 7g. The specific capacitance of five NiCo₂O₄/CNT composites at the same current density is NiCo₂O₄/CNT-4 > NiCo₂O₄/CNT-5 > NiCo₂O₄/CNT-3 > NiCo₂O₄/CNT-2 > NiCo₂O₄/CNT1. This is in agreement with the specific capacitance calculated from the CV curves. It manifests that the specific capacitance of NiCo₂O₄/CNT composites prepared with the addition of different content of SDS can be increased in different degree. The degree of improvement in the specific capacitance are arranged from high to low as follows: NiCo₂O₄/CNT-4 (the addition of 0.864 g of SDS), NiCo₂O₄/CNT-5 (the addition of 1.152 g of SDS), NiCo₂O₄/CNT-3 (the addition of 0.576 g of SDS), NiCo₂O₄/CNT-2 (the addition of 0.288 g of SDS). The reason has been interpreted in the CV curves (Fig. 6f) applied to analyze the specific capacitance of five NiCo₂O₄/CNT composites. The specific capacitance of NiCo₂O₄/CNT1, NiCo₂O₄/CNT-2, NiCo₂O₄/CNT-3, NiCo₂O₄/CNT-4, and NiCo₂O₄/CNT-5 at the current density of 0.5 A g⁻¹ are 285.6, 443.9, 494.7, 574.3 and 496.4 F g⁻¹, respectively. Compared with NiCo₂O₄/CNT-1, the specific capacitance of NiCo₂O₄/CNT-2, NiCo₂O₄/CNT-3, NiCo₂O₄/CNT-4, and NiCo₂O₄/CNT-5 at the current density of 0.5 A g⁻¹ are 1.55, 1.73, 2.01 and 1.74 times, respectively. The specific capacitance of five NiCo₂O₄/CNT composites gradually decrease with the increase of the current density. When compared with the current density of 0.5 A g⁻¹, NiCo₂O₄/CNT-1, NiCo₂O₄/CNT-2, NiCo₂O₄/CNT-3, NiCo₂O₄/CNT-4, and NiCo₂O₄/CNT-5 at the current density of 8 A g⁻¹ exhibit the specific capacitance retention of 87.3%, 78.8%, 87.3%, 75.3%, and 80.2%, respectively. It implies that as-synthesized five NiCo₂O₄/CNT composites possess good rate capability even at a high current density of 8 A g⁻¹, which is a 16-time increase in the current density. The specific capacitance of NiCo₂O₄/CNT-2, NiCo₂O₄/CNT3, NiCo₂O₄/CNT-4, and NiCo₂O₄/CNT-5 at the current density of 8 A g⁻¹ are still larger than that of NiCo₂O₄/CNT-1. The specific capacitance of NiCo₂O₄/CNT-2, NiCo₂O₄/CNT-3, NiCo₂O₄/CNT-4, and NiCo₂O₄/CNT-5 at the current density of 8 A g⁻¹ are 1.40, 1.73, 1.73 and 1.60 times as large as that of NiCo₂O₄/CNT-1, respectively.

Cycling performance of NiCo₂O₄/CNT-1, NiCo₂O₄/CNT-2, NiCo₂O₄/CNT-3, NiCo₂O₄/CNT-4, and NiCo₂O₄/CNT-5 at the current density of 2 A g⁻¹ are presented in Fig. 7h. The specific capacitance of five NiCo₂O₄/CNT composites increase in different degree at the 1000th cycle. At the 1000th cycle, the specific capacitance retention of NiCo₂O₄/CNT-1, NiCo₂O₄/CNT-2, NiCo₂O₄/CNT-3, NiCo₂O₄/CNT-4, and NiCo₂O₄/CNT-5 are 132.7%, 127%, 117.1%, 111.5%, and 114.1%, respectively. It suggests that five NiCo₂O₄/CNT composites exhibit excellent cycling stability.



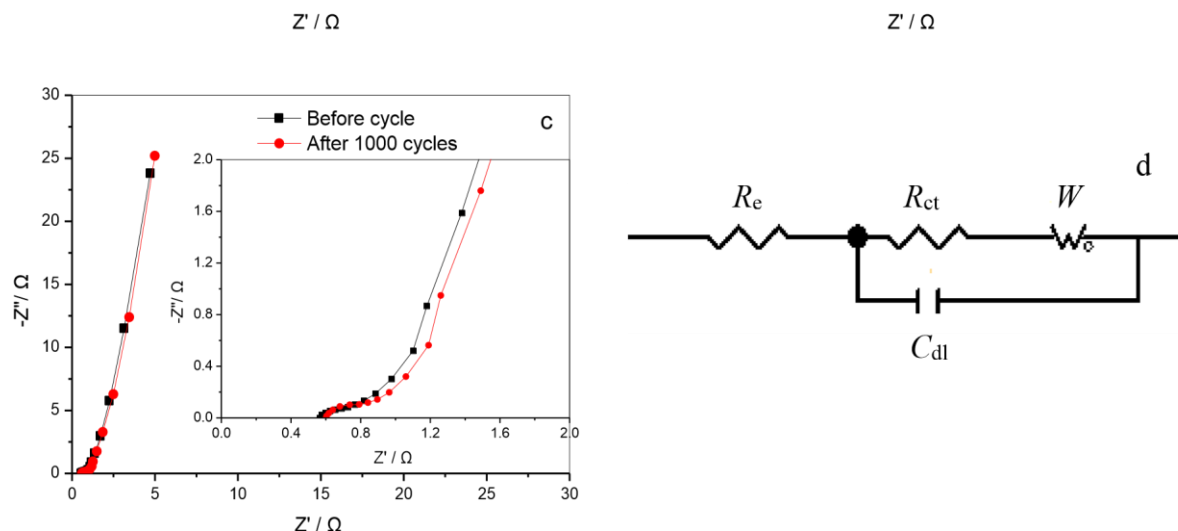


Figure 8. Nyquist impedance plots of NiCo₂O₄/CNT-1 and NiCo₂O₄/CNT-4 measured at 0.1 V before cycles (a); Nyquist impedance plot of NiCo₂O₄/CNT-1 measured at 0.1 V before cycles and after 1000 cycles (b); Nyquist impedance plot of NiCo₂O₄/CNT-4 measured at 0.1 V before cycles and after 1000 cycles (c); A corresponding equivalent circuit for modeling the impedance spectroscopy (d).

Table 1 lists a comparison of the capacitive performance of NiCo₂O₄/CNT-4 with reported ones [19-23, 26]. The specific capacitance of NiCo₂O₄/CNT-4 is relatively low. However, NiCo₂O₄/CNT-4 possesses the best cycling performance (111.5% of initial specific capacitance) and relatively high rate capability. Besides, this work provides an available way to enhance the specific capacitance of NiCo₂O₄/CNT composite synthesized by hydrothermal method with the addition of different content of SDS.

Table 1. Comparison of NiCo₂O₄/CNT composites in literatures with this study.

Preparation method	Specific capacitance	Rate performance	Capacity retention	Reference
Electrochemical deposition	694 F g ⁻¹ (1 A g ⁻¹)	82% (20 A g ⁻¹)	91% (1500 cycles)	[22]
Chemical bath deposition	828 F g ⁻¹ (1 A g ⁻¹)	79% (20 A g ⁻¹)	99% (3000 cycles)	[19]
Chemical bath deposition	828 F g ⁻¹ (1 A g ⁻¹)	79% (20 A g ⁻¹)	99% (3000 cycles)	[20]
Chemical bath deposition	1038 F g ⁻¹ (0.5 A g ⁻¹)	46% (10 A g ⁻¹)	100% (1000cycles)	[21]
Hydrothermal	680 F g ⁻¹ (1 A g ⁻¹)	70.6% (50 A g ⁻¹)	102% (5000 cycles)	[23]
Electrochemical deposition	970 F g ⁻¹ (2 A g ⁻¹)	70% (20 A g ⁻¹)	83% (1000cycles)	[26]
Hydrothermal	574 F g ⁻¹ (0.5 A g ⁻¹)	75.3% (8 A g ⁻¹)	111.5% (1000 cycles)	This work

Fig. 8a displays Nyquist impedance plots of NiCo₂O₄/CNT-1 and NiCo₂O₄/CNT-4 of before cycles. Its equivalent circuit mode is shown in Fig. 8d. Nyquist plots contain a depressed semicircle and a straight line in the high frequency range and in the low frequency range, respectively. In the high frequency range, the point intersecting at the real axis represents a combinational resistance (R_e) containing the active material intrinsic resistance, the electrolyte resistance, and contact resistance at the active material/the current collector interface [35]. Before cycles, R_e values of NiCo₂O₄/CNT-1 and NiCo₂O₄/CNT-4 are 0.31 Ω and 0.57 Ω , respectively. R_e values are low because NiCo₂O₄/CNT-1 and NiCo₂O₄/CNT-4 contain carbon nanotubes with excellent electron conductivity. A depressed semicircle in the high frequency range derives from a parallel combination of the charge-transfer resistance (R_{ct}) and the double-layer capacitance (C_{dl}) [36, 37]. Before cycles, R_{ct} values of NiCo₂O₄/CNT-1 and NiCo₂O₄/CNT-4 are almost equal (around 0.05 Ω). Low R_{ct} value manifests excellent charge-transfer kinetics and easy electron transport, leading to good rate performance of NiCo₂O₄/CNT-1 and NiCo₂O₄/CNT-4 [38]. In the low frequency region, the straight line represents Warburg impedance (W). Fig. 8b and Fig. 8c shows Nyquist impedance plots of NiCo₂O₄/CNT-1 and NiCo₂O₄/CNT-4 before cycles and after 1000 cycles, respectively. Nyquist impedance plots of NiCo₂O₄/CNT-1 before cycles and after 1000 cycles rarely change. Besides, Nyquist impedance plots of NiCo₂O₄/CNT-4 before cycles and after 1000 cycles also almost the same. It demonstrates NiCo₂O₄/CNT-1 and NiCo₂O₄/CNT-4 possess excellent cycle performance. This explains that the specific capacitance of NiCo₂O₄/CNT composites increase rather than decrease after 1000 cycles.

4. CONCLUSIONS

Different content of SDS can affect the morphology and structure of NiCo₂O₄/CNT composites, thus influencing their capacitive performance. The specific capacitance of NiCo₂O₄/CNT composites prepared by adding 0.288 g, 0.576 g, 0.864 g, and 1.152 g of SDS can be increased in different degree when compared with NiCo₂O₄/CNT composite synthesized without the addition of SDS. Among them, NiCo₂O₄/CNT composite synthesized with the addition of 0.864 g of SDS exhibits the highest specific capacitance. Its specific capacitance at 0.5 A g⁻¹ is 574.3 F g⁻¹, which is 2.01 times as large as that of NiCo₂O₄/CNT composites synthesized without the addition of SDS. Besides, NiCo₂O₄/CNT composite with the addition of 0.864 g of SDS exhibits the specific capacitance retention of 75.3% at the current density ranging from 0.5 to 8 A g⁻¹ and initial specific capacitance retention of 111.5% after 1000 cycles, indicating good rate capability and superb cycling stability. Therefore, high specific capacitance, good rate capability and superb cycling stability of NiCo₂O₄/CNT composite with the addition of 0.864 g of SDS promote it as a promising supercapacitor electrode material.

ACKNOWLEDGEMENTS

This work was financially supported by Scientific Research Fund of Hunan Provincial Education Department and Aid Program for Science and Technology Innovative Research Team in Higher Educational Institutions of Hunan Province.

References

1. Y. Li, X. Han, T. Yi, Y. He and X. Li, *J. Energy Chem.*, 31 (2019) 54.
2. R.J. Deokate, R.S. Kalubarme, C.J. Park and C.D. Lokhande, *Electrochim. Acta*, 224 (2017) 378.
3. S.H. Yue, H. Tong, L. Lu, W.W. Tang, W.L. Bai, F.Q. Jin, Q.W. Han, J.P. He, J. Liu and X.G. Zhang, *J. Mater. Chem. A*, 5 (2017) 689.
4. Z.N. Yu, L. Tetard, L. Zhai and J. Thomas, *Energy Environ. Sci.*, 8 (2015) 702.
5. H.G. Wei, H. Wang, A. Li, H.Q. Li, D.P. Cui, M.Y. Dong, J. Lin, J.C. Fan, J.X. Zhang, H. Hou, Y.P. Shi, D.F. Zhou and Z.H. Guo, *J. Alloys Compd.*, 820 (2020) doi: 10.1016/j.jallcom.2019.153111.
6. Z.Z. Zhai, B. Ren, Y.X. Zheng, Y.L. Xu, S.S. Wang, L.H. Zhang and Z.F. Liu, *Chemelectrochem*, 6 (2019) 5993.
7. L.M. Zhao, W.J. Wang, H. Zhao, M. Wang, B. Ge, X. Shao and W.Z. Li, *Appl. Surf. Sci.*, 491 (2019) 24.
8. H.M. Chen, C.Y. Xue, Z.Y. Hai, D.F. Cui, M.X. Liu, Y.K. Li and W.D. Zhang, *J. Alloys Compd.*, 819 (2020) doi: 10.1016/j.jallcom.2019.152939.
9. S. Sahoo, K.K. Naik and C.S. Rout, *Nanotechnology*, 26 (2015) 455401.
10. K. Wang, H.P. Wu, Y.N. Meng and Z.X. Wei, *Small*, 10 (2014) 14.
11. M. Yu, J.P. Chen, J.H. Liu, S.M. Li, Y.X. Ma, J.D. Zhang and J.W. An, *Electrochim. Acta*, 151 (2015) 99.
12. L. Zhang, L. Dong, M. Li, P. Wang, J. Zhang and H. Lu, *J. Mater. Chem. A*, 6 (2018) 1412.
13. C. Liu, W. Jiang, F. Hu, X. Wu and D. Xue, *Inorganic Chemistry Frontiers*, 5 (2018) 835.
14. G.X. Gao, H.B. Wu, S.J. Ding, L.M. Liu and X.W. Lou, *Small*, 11 (2015) 804.
15. W. Qiu, H. Xiao, M. Yu, Y. Li and X. Lu, *Chem. Eng. J.*, 352 (2018) 996.
16. H. Xin, Z. Xu, Y. Liu, W. Li and Z. Hu, *J. Alloys Compd.*, 711 (2017) 670.
17. J. Guo, Z.H. Yin, X.X. Zang, Z.Y. Dai, Y.Z. Zhang, W. Huang and X.C. Dong, *Nano Research*, 10 (2017) 405.
18. F.X. Ma, L. Yu, C.Y. Xu and X.W. Lou, *Energy Environ. Sci.*, 9 (2016) 862.
19. L. Geng, S.S. Xu, J.C. Liu, A.R. Guo and F. Hou, *Electroanalysis*, 29 (2017) 778.
20. S.S. Xu, D.M. Yang, F. Zhang, J.C. Liu, A.R. Guo and F. Hou, *Rsc Advances*, 5 (2015) 74032.
21. F. Cai, Y.R. Kang, H.Y. Chen, M.H. Chen and Q.W. Li, *J. Mater. Chem. A*, 2 (2014) 11509.
22. W.W. Liu, C.X. Lu, K. Liang and B.K. Tay, *J. Mater. Chem. A*, 2 (2014) 5100.
23. S. Abouali, M.A. Garakani, Z.L. Xu and J.K. Kim, *Carbon*, 102 (2016) 262.
24. X.C. Li, W. Sun, L.Q. Wang, Y.D. Qi, T.M. Guo, X.H. Zhao and X.B. Yan, *Rsc Advances*, 5 (2015) 7976.
25. J. Wu, P. Guo, R. Mi, X.C. Liu, H. Zhang, J. Mei, H. Liu, W.M. Lau and L.M. Liu, *J. Mater. Chem. A*, 3 (2015) 15331.
26. M. Oguntoye, S. Oak, L. Pashazanusi, L. Pratt and N.S. Pesika, *Electrochim. Acta*, 236 (2017) 408.
27. M.S. Wu, Z.B. Zheng, Y.S. Lai and J.J. Jow, *Electrochim. Acta*, 182 (2015) 31.
28. Y. Li and X. Peng, *ChemistrySelect*, 2 (2017) 8959.
29. N. Wang, B.L. Sun, P. Zhao, M.Q. Yao, W.C. Hu and S. Komarneni, *Chem. Eng. J.*, 345 (2018) 31.
30. Y. Xue, T. Chen, S. Song, P. Kim and J. Bae, *Nano Energy*, 56 (2019) 751.
31. Y.H. Li, S.Y. Zhang, Q.Y. Chen and J.B. Jiang, *Int. J. Electrochem. Sci.*, 10 (2015) 6199.

32. Y.H. Li, K.L. Huang, D.M. Zeng, S.Q. Liu and Z.F. Yao, *J. Solid State Electrochem.*, 14 (2010) 1205.
33. X. Yu, B. Lu and Z. Xu, *Adv. Mater.*, 26 (2014) 1044.
34. Y.H. Li, K.L. Huang, S.Q. Liu, Z.F. Yao and S.X. Zhuang, *J. Solid State Electrochem.*, 15 (2011) 587.
35. W.L. Yang, Z. Gao, J. Ma, J. Wang, B. Wang and L.H. Liu, *Electrochim. Acta*, 112 (2013) 378.
36. Y.H. Li, K.L. Huang, Z.F. Yao, S.Q. Liu and X.X. Qing, *Electrochim. Acta*, 56 (2011) 2140.
37. Q. Guan, J.L. Cheng, B. Wang, W. Ni, G.F. Gu, X.D. Li, L. Huang, G.C. Yang and F.D. Nie, *ACS Appl. Mater. Interfaces*, 6 (2014) 7626.
38. H. Che, A. Liu, J. Mu, Y. Bai, C. Wu, X. Zhang, Z. Zhang and G. Wang, *Electrochim. Acta*, 225 (2017) 283

© 2020 The Authors. Published by ESG (www.electrochemsci.org). This article is an open access article distributed under the terms and conditions of the Creative Commons Attribution license (<http://creativecommons.org/licenses/by/4.0/>).